Available online at www.sciencedirect.com

ScienceDirect

Underground Space 28 (2026) 332–349

www.keaipublishing.com/undsp

Case Report

TBM performance assessment for the BBT exploratory tunnel in the Central Gneiss unit

Deniz Aydin [a], Francesco Tinti [b], Daniela Boldini [c,*]

[a] Department of Mining Engineering, Dicle University, Diyarbakir 21280, Turkey
[b] Department of Civil, Chemical, Environmental, and Materials Engineering, University of Bologna, Bologna 40131, Italy
[c] Department of Chemical Engineering Materials Environment, Sapienza University of Rome, Roma 00184, Italy

Received 10 August 2025; received in revised form 19 January 2026; accepted 2 February 2026
Available online 20 April 2026

Abstract

Tunnel boring machines (TBMs) have become essential in modern tunnelling projects due to their efficiency, safety, and ability to manage complex geological conditions. Accurate prediction of TBM performance is critical for project planning, risk management, and cost estimation. This study focuses on the performance assessment of a hard rock double-shield TBM used in the exploratory tunnel of the Brenner Base Tunnel (BBT) underground system, specifically within the Central Gneiss unit. Several prediction models from the literature, including those based on rock mass classification systems such as RMR and GSI, were applied and compared with actual TBM performance data collected over approximately 3200-m stretch. The relationships between TBM operational parameters, such as penetration rate, instantaneous cutting rate, specific energy, boreability index, power consumption, specific penetration, and geomechanical properties were statistically analysed. Two new predictive models based on RMR and GSI were also proposed and evaluated. The results demonstrate good correlations between rock mass quality indices and TBM performance indicators, highlighting the importance of detailed geomechanical characterisation for reliable performance forecasting.

Keywords: TBM tunnelling; Performance prediction model; Rock mass classification; Central gneiss; Brenner Base Tunnel

1 Introduction

Tunnel boring machines (TBMs) have become an indispensable tool in modern tunnelling projects due to their efficiency, safety, and ability to traverse complex geological conditions. With the growing demands of urbanisation and infrastructure development, TBMs are now extensively employed in various sectors, including transportation, water conveyance, and hydropower schemes. In long tunnelling projects in rock, TBMs offer several advantages over conventional drill and blast methods, such as higher excavation rates, reduced environmental impact, and safer working conditions (She et al., 2024; Yan et al., 2024). Furthermore, TBMs ensure consistent tunnel profiles with minimal deviation, making them particularly suitable for long and deep tunnels under variable geological conditions (Goodarzi et al., 2021).

The success of a TBM project heavily depends on the accurate prediction of its performance, which is influenced by a complex interplay of factors, including rock mass properties, machine specifications, and operational parameters. These factors vary significantly across projects, making TBM performance prediction a challenging yet essential task (Salimi et al., 2022). Parameters such as penetration rate (PR), advance rate (AR), and cutter wear significantly affect project timelines, costs, and risk management (Naghadehi et al., 2018; Armaghani et al., 2021). Consequently, developing and applying TBM performance prediction models have become critical components of project planning and decision-making processes (Entacher & Rostami, 2019; Yalei et al., 2024).

* Corresponding author.
E-mail address: daniela.boldini@uniroma1.it (D. Boldini).
Peer review under the responsibility of Tongji University

https://doi.org/10.1016/j.undsp.2026.02.006

List of symbols and acronyms used in the paper

AR	advance rate (m/h)
BBT	Brenner Base Tunnel
BI	Boreability index (kN/cutter)/(mm/rev)
BTC	Brenner Tunnel Construction
CAI	Cerchar abrasivity index
D_{TBM}	TBM diameter (m)
d_c	cutter diameter (mm)
DRI	drilling rate index
ET	exploratory tunnel
F_N	normal force per cutter (kN/cutter)
FPI	field penetration index (kN/cutter)/(mm/rev)
GSI	geological strength index
ICR	instantaneous cutting rate (m^3/h)
J_c	condition of the joints
k	energy transfer coefficient (typically ranging in the interval 0.8–0.9 for TBM)
k_1	correction factor for specific failure energy
k_2	correction factor for spacing and orientation of discontinuities
k_3	correction factor state of stress
k_4	correction factor for cutter diameters ≠ 432 mm
k_5	correction factor for cutter spacing
MT-E	east main tunnel
MT-W	west main tunnel
ML	machine learning
n_c	number of cutters
P	power consumption (kW)
PR	penetration rate (mm/rev)
R^2	determination coefficient
RMR	rock mass rating
RMSE	root mean square error
RQD	rock quality designation
RSR	rock structure rating
RT_c	rock type code
s_c	average cutter spacing (mm)
SE	specific energy (kWh/m^3)/(MJ/m^3)
SP	specific penetration (mm/rev)/(kN/cutter)
TBM	tunnel boring machine
UCS	uniaxial compressive strength of the intact rock (MPa)
UCS_m	uniaxial compressive strength of the rock mass (MPa)
v_{rot}	cutterhead rotational speed (rpm)
W_f	failure energy (N·m)
w_f	specific failure energy ($m^3 \times 10^{-6}$)
α	angle between the discontinuities and the tunnel axis (°)

The control and prediction of TBM performance are fundamental aspects of tunnelling projects, as they directly impact machine selection, project scheduling, and budgeting. Accurate performance estimation enables engineers to optimize machine parameters, reduce operational risks, and anticipate potential challenges arising from geological variability (Jing et al., 2019). This activity plays a vital role in assessing the economic feasibility of using TBMs in tunnelling projects by estimating costs associated with machine operation, cutter replacement, and potential delays (Hassanpour et al., 2011).

TBM performance prediction methods can be broadly classified into three categories: theoretical, empirical, and machine learning-based approaches. Each category has its own strengths and limitations, making it suitable for different project requirements and geological conditions.

Theoretical models are based on the principles of rock mechanics and cutting mechanics. These models analyse the interaction between the TBM cutter and the rock mass to estimate cutting forces, penetration rates, and energy consumption. One of the most widely recognised theoretical models is the one developed at the Colorado School of Mines (CSM), which calculates cutter forces based on rock properties such as uniaxial compressive strength (UCS) and tensile strength (Rostami & Ozdemir, 1993). Although theoretical models provide valuable insights into the mechanics of rock cutting, they occasionally fail to account for the variability and complexity of in-situ geological conditions, such as joint spacing, orientation, and weathering (Hamidi et al., 2010). To address these limitations, researchers have introduced modifications to incorporate rock mass properties, such as the inclusion of joint-related parameters to the CSM model (Yagiz, 2003). Another well-known theoretical model is the one by Gehring (1995), in which a base equation correlates PR with UCS and cutter load. The latest version of the model introduced five correction factors, accounting for fracture energy, joint spacing, stress state, cutter diameter, and cutter spacing, all derived from empirical correlations. Additionally, an empirical equation was included for predicting cutter wear based on the Cerchar abrasivity index (CAI) (Brino et al., 2015; Entacher & Rostami, 2019).

Empirical models rely on field data collected from previous tunnelling projects to establish statistical correlations between TBM performance and geomechanical or operational parameters. These models are often preferred for their simplicity and ease of application, especially during the early stages of project planning. The model developed at the Norwegian University of Science and Technology (NTNU), for example, uses rock mass classification systems such as the rock quality designation (RQD) and the

drilling rate index (DRI) to predict PR (Bruland, 1998). Similarly, the field penetration index (FPI) model, developed by Nelson et al. (1983) and later refined by Hassanpour et al. (2011), correlates cutter load and penetration per revolution with rock mass parameters such as UCS of intact rock and joint spacing. Many of the rock mass properties used in predicting TBM performance are directly linked to the input parameters of rock mass classification systems. As a result, several researchers have investigated the relationship between TBM performance and classification systems, including the Q-system, rock mass rating (RMR), rock structure rating (RSR) and geological strength index (GSI) (Cassinelli et al., 1982; Innaurato et al., 1991; Barton, 1999; Alber, 2000; Sapigni et al., 2002; Ribacchi & Lembo-Fazio, 2005; Hassanpour et al., 2011; Hamidi et al., 2010; Frough et al., 2015; Benato & Oreste, 2015; Liu et al., 2017; Pourhashemi et al., 2021; She et al., 2024).

In recent years, machine learning (ML) techniques have emerged as a promising approach for TBM performance prediction. These methods leverage large datasets and advanced algorithms to identify complex patterns and relationships between input parameters and performance indicators. Techniques such as artificial neural network (ANN), support vector machine (SVM), and random forests have been successfully applied to predict PR and AR under various geological and geomechanical conditions (Ayawah et al., 2022). Moreover, ML approaches have been extended to rock mass classification and cutter wear analysis, enhancing the precision of TBM performance predictions. For instance, bimodal feature fusion frameworks utilising TBM operational parameters and cutter wear data have achieved high accuracy in rock mass classification (Yang et al., 2025a). Additionally, improved boreability indices for gripper TBMs in medium- to strong-quality rocks have been proposed, based on theoretical analysis and field penetration tests, to eliminate the influence of operational parameters and provide more reliable performance predictions (Yang et al., 2025b).

Beyond TBM performance, ML techniques have also been applied to predict geomechanical properties of rock materials, which are critical for safe design in geoengineering projects. SVM models have shown impressive results in predicting UCS for limestone (Cemiloglu et al., 2023). Similarly, deep learning methods, such as deep neural network (DNN), have been employed to predict index mechanical properties and strength parameters of marlstone for various geotechnical indices, specifically UCS, angle of internal friction, bulk modulus, and P-wave modulus (Azarafza et al., 2022). These advancements in ML and deep learning underscore their potential as complementary tools for enhancing the reliability of geotechnical assessments and TBM performance forecasting.

The present research provides an original contribution by reviewing and comparing the performance of existing empirical models while proposing new predictive relationships between measured operational TBM data and both RMR and GSI values from the Brenner Base Tunnel (BBT) case study in Italy. Specifically, the performance of the TBM used during the excavation of the exploratory tunnel in the Central Gneiss unit was analysed to gain deeper insight into its behaviour under the specific geological and geomechanical conditions. This study serves as a guiding framework for tunnels excavated in gneiss, which exhibits high strength and abrasiveness.

While similar to numerous prior studies, the data utilized in this research are based on specific geological and geomechanical conditions and a limited dataset. A key distinction of this work lies in the validation of the proposed penetration rate models for the main tunnels. Despite their larger diameters and the different TBM employed compared to the exploratory tunnel, the successful application of the models from the exploratory tunnel to the main tunnels enhances the generalizability of the findings, particularly for the gneiss rock mass and for projects involving the use of exploratory tunnels. Consequently, this research makes a significant theoretical contribution while also providing an important reference for practical applications in exploratory tunnelling.

2 Tunnel description

The BBT is a 55 km-long railway tunnel project that will connect Fortezza (Italy) and Innsbruck (Austria) once completed. The excavation crosses the Eastern Alps beneath a variable overburden reaching up to 1700 m. The entire tunnel system extends over 230 km and includes the exploratory tunnel (ET), the two main tunnels, East (MT-E) and West (MT-W), as well as cross passages, emergency stations, and access tunnels.

2.1 Description of the tunnel case study

The exploratory tunnel, already completed, was chosen as the case study for the present work. It was excavated using a double-shield TBM with a diameter of 6.85 m and is located between the two main tunnels, approximately 12 m deeper. Its purpose was to investigate the geological and geomechanical conditions in advance of the excavation of the other two tunnels. Once the infrastructure is completed and operational, the ET will be used for water drainage and maintenance during tunnel system operation (Boldini et al., 2018), and potentially for research purposes (Tinti et al., 2023). In contrast, the two main tunnels, MT-E and MT-W, were excavated using twin double-shield TBMs with a diameter of 10.71 m (Egger et al., 2023).

2.2 Geological and geomechanical conditions

The tunnels were excavated under highly complex geological and geomechanical conditions, encompassing several distinct zones and fault lines (Egger et al., 2023). This study focuses on the performance of the ET within

the Central Gneiss unit, which is primarily classified as "good" and secondarily as "fair" in terms of rock mass quality, according to Bieniawski's classification (i.e., classes II and III, respectively). This unit consists of mica, schist, quartz, and feldspar, and is characterised by high strength and abrasiveness of the intact rock, as indicated by the geological forecast model.

During the design phase, estimates and forecasting models were developed by BBT to characterise the rock mass along the tunnel alignment (Maggio et al., 2022). Additionally, during the excavation of the exploration tunnel, around 150 boreholes, 100 m long, were drilled approximately every 100 m from the head of the TBM. Both destructive drilling and sample recovery were applied, and water flow rate and hydraulic pressure were collected, too. The surveys gathered critical information, including advance speed, thrust, rotational speed, torque, rotational pressure, and specific energy. Following the completion of each drilling, an optical televiewer survey was conducted to examine the borehole walls in detail. Simultaneously, seismic tests were performed to analyze the propagation of P and S seismic waves, helping to identify potential fault zones or areas of poor-quality material.

In addition, periodic rock mass surveys were carried out during the excavation by geologists from both the Site Supervision Team of the Client (BBT) and the contractor, Brenner Tunnel Construction (BTC), leading to the determination of GSI and RMR ratings presented in Fig. 1. The sampling interval ranges from 9 to 178 m, with an average value of 58.5 m. Additionally, UCS tests on rock samples from radial drillings were conducted by the laboratory of the Technical University of Munich. The results of the UCS tests and RQD values are shown in Fig. 2. Finally, Fig. 3 shows the specific tunnel stretch, chainage, and geological features of the analysed area.

2.3 Characteristics of the TBM

The ET excavation was performed using a Herrenknecht hard rock TBM (Model S-1054). The main technical features of the machine are summarised in Table 1. Figure 4, obtained using TBM data at the points where RMR and GSI scores were determined, presents the variations in the operational parameters of the TBM, including thrust force, PR, torque, and cutterhead rotational speed, along the ET within the Central Gneiss unit. Analysis of the data reveals a relationship between TBM performance and the geomechanical properties of the rock mass. In sections where the rock mass exhibits higher UCS, RMR, RQD, and GSI, the TBM operates under increased mechanical loads, requiring greater thrust force and exhibiting higher torque in response. However, under these conditions, both the PR and the cutterhead rotational speed are reduced, indicating slower progress through more competent and intact rock mass. Conversely, in sections where the rock mass is weaker and more fractured, characterised by lower values of the geomechanical indices, the TBM requires less thrust, while measured and torque values decrease, and higher penetration rates and cutterhead rotation speeds are observed.

3 Methodology

First, existing TBM performance prediction models were applied, and their estimated results for the ET were compared with the actual penetration rates recorded by the TBM. Error analyses were then conducted to identify the models providing the most accurate predictions. Subsequently, correlations between the TBM operational parameters, including PR, power consumption (P), and specific penetration (SP), and the geomechanical indices (RMR and GSI values) were investigated. In addition, derived parameters, including instantaneous cutting rate (ICR), specific energy (SE), and boreability index (BI), were calculated using the following formulas to provide further insight into TBM performance:

$$\mathrm{SE} = \frac{4 \cdot 1000 \cdot P}{\mathrm{PR} \cdot v_{\mathrm{rot}} \cdot 60 \cdot \pi \cdot D_{\mathrm{TBM}}^2} \quad (1)$$

(Bilgin et al., 2014),

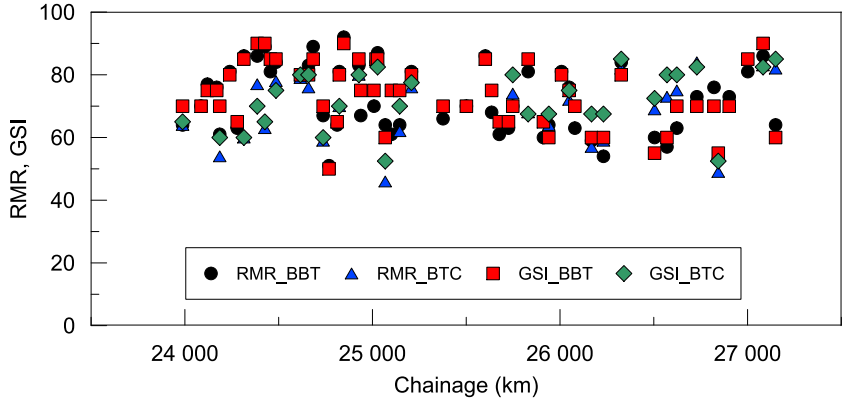

Fig. 1. GSI and RMR ratings collected during the excavation of the ET within the Central Gneiss unit.

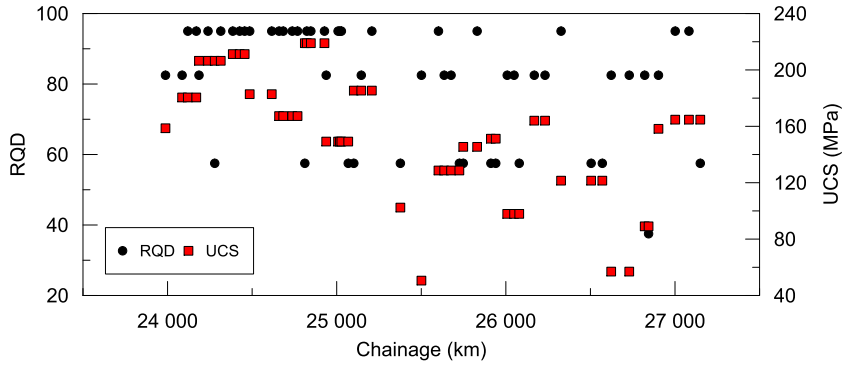

Fig. 2. UCS test results and RQD values from the ET within the Central Gneiss unit.

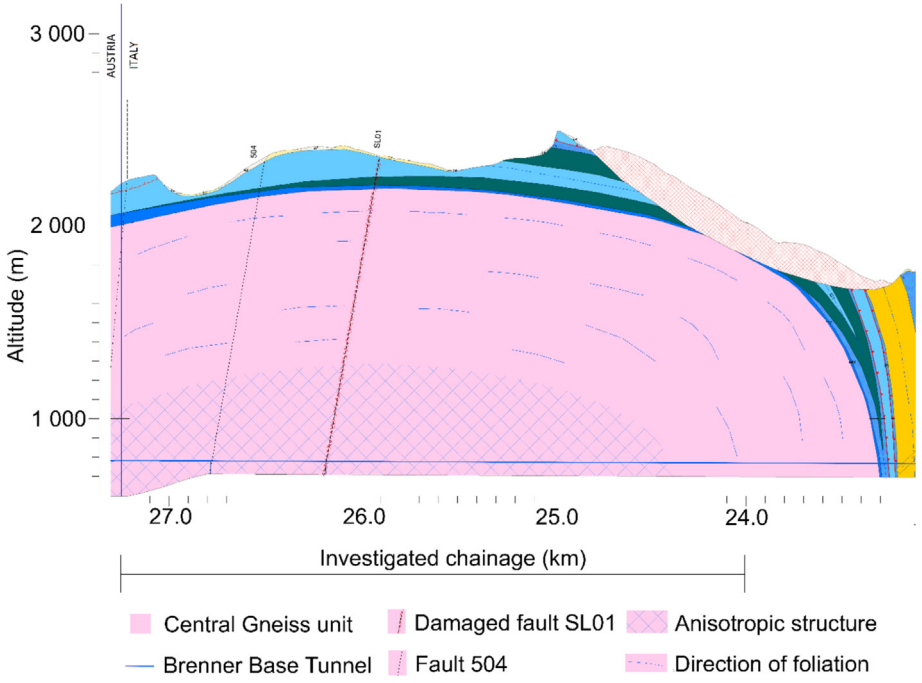

Fig. 3. Geological cross-section of the tunnel alignment within the Central Gneiss unit analysed in this study.

$$\mathrm{ICR} = k \cdot \frac{P}{\mathrm{SE}} \tag{2}$$

(Exadaktylos et al., 2008),

$$\mathrm{BI} = \frac{F_\mathrm{N}}{\mathrm{PR}} \tag{3}$$

(Hamidi et al., 2010), where P is the power consumption, v_rot the cutterhead rotational speed, D_TBM the TBM diameter, and F_N the normal force per cutter.

Finally, two new predictive models were proposed based on these analyses.

3.1 Selection of performance prediction models

In selecting the performance prediction models for this study, particular attention was given to their limitations and domains of applicability, with preference accorded to methods incorporating rock mass and intact rock indices, such as RMR, GSI, and UCS. The limitations of the selected models, along with the typical ranges of TBM and rock mass parameters for the BBT project, are summarised in Table 2. With regard to the latter, UCS values were obtained from laboratory tests on rock samples, while RMR values were derived by integrating laboratory measurements with field observation. Eq. (4) was used to calculate the UCS value of the rock mass ($\mathrm{UCS_m}$), while Eq. (5) was used to calculate the RSR:

$$\mathrm{UCS_m} = \mathrm{UCS} \cdot \sqrt{\exp\left(\frac{\mathrm{RMR} - 100}{18}\right)}, \tag{4}$$

$$\mathrm{RSR} = 0.77 \cdot \mathrm{RMR} + 24. \tag{5}$$

The values of TBM diameter (D_TBM), average cutting space (s_c), cutter diameter (d_c), number of cutters (n_c), cut-

Table 1
Technical specifications of the TBM used for the excavation of the ET (Egger et al., 2023).

Technical specifications	S-1054 (ET)
Machine length/weight	270 m/1300 t
Main drive power	2800 kW
Thrust main cylinders (number)	42 750 kN (10)
Thrust auxiliary cylinders (number)	57 000 kN (16)
Shield + Cutterhead length	12 000 mm
Conicity/Extended overbore	95 mm/224 mm
Cutterhead boring diameter	6850 mm
Cutterhead rotational speed	0–9.05 rpm (Range I) 0–4.50 rpm (Range II)
Nominal torque	5247 kN·m (Range I) 10 574 kN·m (Range II)
Number of cutters	41
Diameter of cutters	19″ (482.6 mm)
Spacing between cutters	90 mm
Contact thrust/Load per cutter	13 000 kN / 317 kN

terhead rotational speed (v_{rot}), and the normal force per cutter (F_N) were obtained from Egger et al. (2023).

The models proposed by Cassinelli et al. (1982), Ribacchi and Lembo Fazio (2005), Hassanpour et al. (2011), and Farrokh et al. (2012) were selected due to the lithological similarities between their original application contexts and the Central Gneiss unit. In particular, the model of Cassinelli et al. (1982) was considered suitable for the RSR and UCS of the rock mass ranges encountered in the study area. The models of Innaurato et al. (1991), Gehring (1995), and Farrokh et al. (2012) were included based on their compatibility with the UCS values recorded along the tunnel alignment, while the Hamidi (2010) model was considered appropriate with reference to the mean UCS values observed. Additionally, the models proposed by Ribacchi and Lembo Fazio (2005), Hassanpour et al. (2011), Frough et al. (2015), and Kim et al. (2020) were selected due to their consistency with the RMR ranges identified in the Central Gneiss unit. The selected models are summarised in Table 3.

3.2 Data analysis for GSI and RMR

RMR and GSI values, obtained from 55 different locations, were correlated with the corresponding TBM operational data, recorded as average values over excavation advance. For the analysis, the chainage points with RMR and GSI estimates were treated as midpoints, and different excavation advance lengths were tested to check the best correlation. Specifically, advances ranging from approximately 1.5 to 15 m were evaluated. Since RMR and GSI results were very similar across different advance lengths, all subsequent analyses were conducted considering the single excavation advance (i.e., of approximately 1.5 m) covering the midpoint.

Due to the presence of numerous repeated values in both the RMR and GSI datasets, a data regularization process was applied. Five-unit class intervals were defined between 50 and 100 for both RMR and GSI values. The average TBM data within each interval was then calculated, reducing the total number of data points and enabling a more effective statistical analysis. The raw dataset contained 55 data points for both RMR and GSI, while the regularized dataset was reduced to 9 data points for each. Data were grouped into intervals of width 5 for both RMR and GSI. Table 4 represents the distribution of RMR and GSI data across these intervals, showing the number of data points in each range. Each interval is represented by a single data point in the regularised dataset.

Subsequent correlations were performed using this processed dataset. Figure 5 shows an example of the correlation trends obtained from the raw dataset (open circles) and the averaged dataset (solid circles). The analysis of the raw data yielded a correlation coefficient of $R^2 = 0.41$, whereas the regularized dataset resulted in a significantly higher correlation coefficient of $R^2 = 0.83$. This demonstrates that the statistical analysis based on the regularized dataset produces higher correlation coefficients and stronger regression models, facilitating the interpretation of the influence of rock mass properties on TBM performance.

3.3 Statistical analysis

The predictive performance of the selected models was evaluated using the coefficient of determination (R^2), the correlation coefficient (ρ), and the root mean square error (RMSE), which together provide a measure of the strength of the correlation between predicted and observed values as well as the associated prediction error. Observed penetration values that occurred multiple times were grouped, and the corresponding model predictions were averaged to maintain consistency within the dataset. For each model, both linear and polynomial regression analyses were carried out to assess predictive capability.

4 Results and discussion

4.1 Results from the prediction models

To allow for a consistent comparison between the penetration values expressed in various units by the different models and those recorded by the TBM in millimeters per revolution (mm/rev), appropriate unit conversions were carried out for each excavation advance (Table 5). These conversions were based on the corresponding average values of normal force per cutter and cutterhead rotational speed.

Table 6 reports the mean measured penetration rates from the Northern Italian stretch of the Brenner Base exploratory tunnel, within the approximate length of

Table 2
Limitations of the selected models and parameter ranges for the TBM and rock mass considered in the BBT project.

Model	Database	Lithology	TBM and rock mass parameters	BBT project parameters
Gehring (1995)	Based on 4 projects: 2 in South Africa and 2 in South Korea	Igneous, metamorphic, and sedimentary rocks	UCS = 100–250 MPa s_c = 80 mm d_c = 17 mm F_N = 200 kN	UCS = 50–218 MPa $UCS_{(mean)}$ = 155 MPa UCS_m = 20–175 MPa $UCS_{m(mean)}$ = 77 MPa RMR = 51–92 RMR_{mean} = 76 RSR = 51–83 D_{TBM} = 6.85 m s_c = 90 mm d_c = 19 mm n_c = 41 v_{rot} = 4.9–6.1 rpm F_N = 98–221 kN
Cassinelli et al. (1982)	1898 m of tunnel excavation with a section of 5.2 m^2	Biotite embrechites and anatexites alternate, quartzitic gneiss with biotite	UCS_m = 34–149 MPa $UCS_{m(mean)}$ = 97 MPa RSR = 60–95 D_{TBM} = 2.57 m	
Innaurato et al. (1991)	19 km of tunnels	Igneous, sedimentary, and metamorphic rocks	UCS = 50–150 MPa	
Ribacchi and Lembo Fazio (2005)	6.6 km of hydraulic tunnel	Orthogneiss composed of quartz, feldspar and mica; mica content (mostly biotite) is in the 10%–20% range	UCS = 100–200 MPa $UCS_{(mean)}$ = 160 MPa RMR = 65–100 D_{TBM} = 3.84 m	
Hamidi et al. (2010)	Zagros long water conveyance tunnel project with 48 km total length in western Iran	Mainly sedimentary rocks, shale and limestone, with rapid changes from good to poor conditions (hard and soft rock, water flows varied very quickly, mixed faces are present)	UCS = 20–150 MPa $UCS_{(mean)}$ = 130 MPa RMR = 20–60 RMR_{mean} = 40 D_{TBM} = 6.73 m N_c = 43 s_c = 90 mm	
Hassanpour et al. (2011)	Three Iranian projects and one tunnel in New Zealand, with a total length of 56.4 km	Limestone, shale and sandstone, slate, phyllite, schist with quartzitic veins, tuffs, agglomerate, gneiss, intrusive rocks	UCS = 15–225 MPa D_{TBM} = 4.53–10.05 m RMR = 20–85	
Farrokh et al. (2012)	17 different projects, with a variability of conditions and TBM parameters with a total length of 73.6 km	Limestone, shale and sandstone, slate, phyllite, schist with quartzitic veins, tuffs, agglomerate, gneiss intrusive rocks, dolomite, argillite, granite	UCS = 10–250 MPa D_{TBM} = 3.84–11.8 m v_{rot} = 6–11 rpm	
Frough et al. (2015)	30-km long water conveyance tunnel	Variety of pyroclastic rocks, often interbedded with sedimentary rocks. The characteristic rock types are green vitric to crystal lithic tuff, tuff breccias, sandy and silty tuffs with shale, siltstone and sandstone	UCS = 15–150 MPa $UCS_{(mean)}$ = 91 MPa RMR = 21–75 RMR_{mean} = 53 D_{TBM} = 4.66 m	
Kim et al. (2020)	2.258 m electric power tunnel	Precambrian biotite banded gneiss and some intrusive rocks	UCS = 22–97 MPa $UCS_{(mean)}$ = 53.9 MPa RMR = 49–84 RMR_{mean} = 67 D_{TBM} = 3.3 m	

3200 m, in the Central Gneiss unit between chainages km 23 + 988 and 27 + 273, and the mean values predicted by each model at the same range, all expressed in mm/rev. Hassanpour et al. (2011) presented three different relationships to obtain the FPI and then PR: one based on UCS and RQD, the second based on RMR and the last based on GSI (See Table 3). In Table 6, the PR results are reported for all three relationships.

A comparison between measured and predicted PR reveals significant differences in the performance of the various empirical models (Fig. 6). Most models, including those proposed by Gehring (1995), Cassinelli et al. (1982), Innaurato et al. (1991), Ribacchi and Lembo Fazio (2005), Hamidi et al. (2010), and Farrokh et al. (2012), consistently underestimate the recorded values, with data points clustering below the 1:1 reference line. Similarly, Hassanpour et al. (2011) model, based on UCS and RQD, as well as the one based on GSI, shows a marked tendency to under predict, accompanied by considerable data scatter, indicating limited reliability. By

Table 3
Overview of the selected performance prediction models for the ET.

Model	Main equations
Cassinelli et al. (1982)	$PR = -0.0059 \cdot RSR + 1.59$ $RSR = 0.77 \cdot RMR + 12.4$
Innaurato et al. (1991)	$PR = 40.41 \cdot UCS^{-0.437} - 0.047 \cdot RSR + 3.15$
Gehring (1995)	$PR = \frac{4 \cdot F_N}{UCS} \cdot k_1 \cdot k_2 \cdot k_3 \cdot k_4 \cdot k_5$ (see Appendix A) $k_1 = 0.475 \cdot w_f^{-0.56}$ with $w_f = \frac{W_f}{UCS}$ $k_2,\ k_3,\ k_5,\ k_4 = \frac{432}{d_c}$
Ribacchi and Lembo Fazio (2005)	$SP = 250 \cdot UCS_m^{-0.66}$ $UCS_m = UCS \cdot \sqrt{e^{\frac{RMR-100}{18}}}$
Hamidi et al. (2010)	$FPI = 9.401 + 0.397 \cdot \log \alpha + 0.011 \cdot J_c^2 + 1.14 \cdot 10^{-5} \cdot RQD^3 + 1.32 \cdot 10^{-8} \cdot UCS^4$
Hassanpour et al. (2011)	$FPI = 0.053 \cdot RMR^2 - 4.205 \cdot RMR + 92.068$ $FPI = 4.619 \cdot \exp(0.023 \cdot GSI)$ $FPI = \exp(0.008 \cdot UCS + 0.015 \cdot RQD + 1.384)$
Farrokh et al. (2012)	$PR = \exp\left(\begin{array}{c} 0.41 + 0.404 \cdot D_{TBM} - 0.027 \cdot D_{TBM}^2 + 0.0691 \cdot RT_c + \\ -0.00431 \cdot UCS + 0.0902 \cdot RQD + 0.0893 \cdot F_N \end{array}\right)$ (see Appendix B for RT_c)
Frough et al. (2015)	$AR = -0.0004 \cdot RMR^2 + 0.055 \cdot RMR + 1.98$
Kim et al. (2020)	$FPI = 0.0471 \cdot SE^2 + 0.4004 \cdot SE + 6.9643$

Table 4
Distribution of RMR and GSI data across defined intervals.

Range	Number of RMR data	Number of GSI data
50–54	3	1
55–59	2	2
60–64	15	6
65–69	4	5
70–74	6	12
75–79	4	8
80–84	13	7
85–89	7	10
90–94	1	4
Total	55	55

contrast, the version of the Hassanpour et al. (2011) model incorporating the RMR parameter exhibits closer agreement, with predictions aligning more closely with the measured values. The models developed by Frough et al. (2015) and Kim et al. (2020) display a broader spread, with both under- and overestimations, yet overall demonstrate a stronger correlation with the actual data. These findings highlight the inherent challenges in accurately modelling TBM penetration rates using empirical approaches.

The discrepancy between measured and predicted values was evaluated using the RMSE and the correlation coefficient (ρ). The results are presented in Table 7 and Fig. 7.

The inspection of the graphs reveals that six out of the eleven models exhibit negative correlations. This indicates that, despite having relatively comparable RMSE values, these models fail to accurately predict the outcomes, as their predictions are inversely related to the measured values (i.e., higher measured values correspond to lower predicted values). In contrast, the remaining five models display positive correlations. Among these, the models by Cassinelli et al. (1982), Innaurato et al. (1991), and Hassanpour et al. (2011) (RMR-based) demonstrate the lowest RMSE values, suggesting better predictive accuracy. On the other hand, the models by Frough et al. (2015) and Kim et al. (2020) show the highest RMSE values; therefore, despite their positive correlations, their overall predictive performance remains unsatisfactory. It is essential to establish whether the errors associated with each model are random or follow a systematic pattern. This aspect is examined in greater detail in the following section.

4.2 Regression analysis of the error

Measured PR and those calculated, from the empirical TBM models were compared using regression analyses (linear and second-order polynomial). This enabled calculation of statistical indicators reflecting the error behaviour: the coefficient of determination (R^2) and RMSE. The results are presented in Table 8 and Fig. 8. The comparison reveals notable differences in error behaviour among the models. Generally, polynomial regression significantly improves both R^2 and RMSE values for most models. For this reason, subsequent analyses were based on polynomial regression results.

The comparative analysis of the prediction models, as illustrated in Fig. 8, reveals significant differences in their error behaviour regarding TBM penetration rates. Models such as Cassinelli et al. (1982), Kim et al. (2020), and Ribacchi and Lembo Fazio (2005) are located in the upper-left quadrant (Quadrant 1), where both high R^2 and low RMSE values are observed. This indicates that the error produced by these models exhibits a systematic behaviour. In contrast, models such as Frough et al. (2015), Hamidi et al. (2010), Hassanpour et al. (2011) (UCS and RQD), and Gehring (1995) are positioned in the upper-right quadrant (Quadrant 2). These models are characterised by relatively high R^2 and RMSE values. The error behaviour remains systematic, although the data

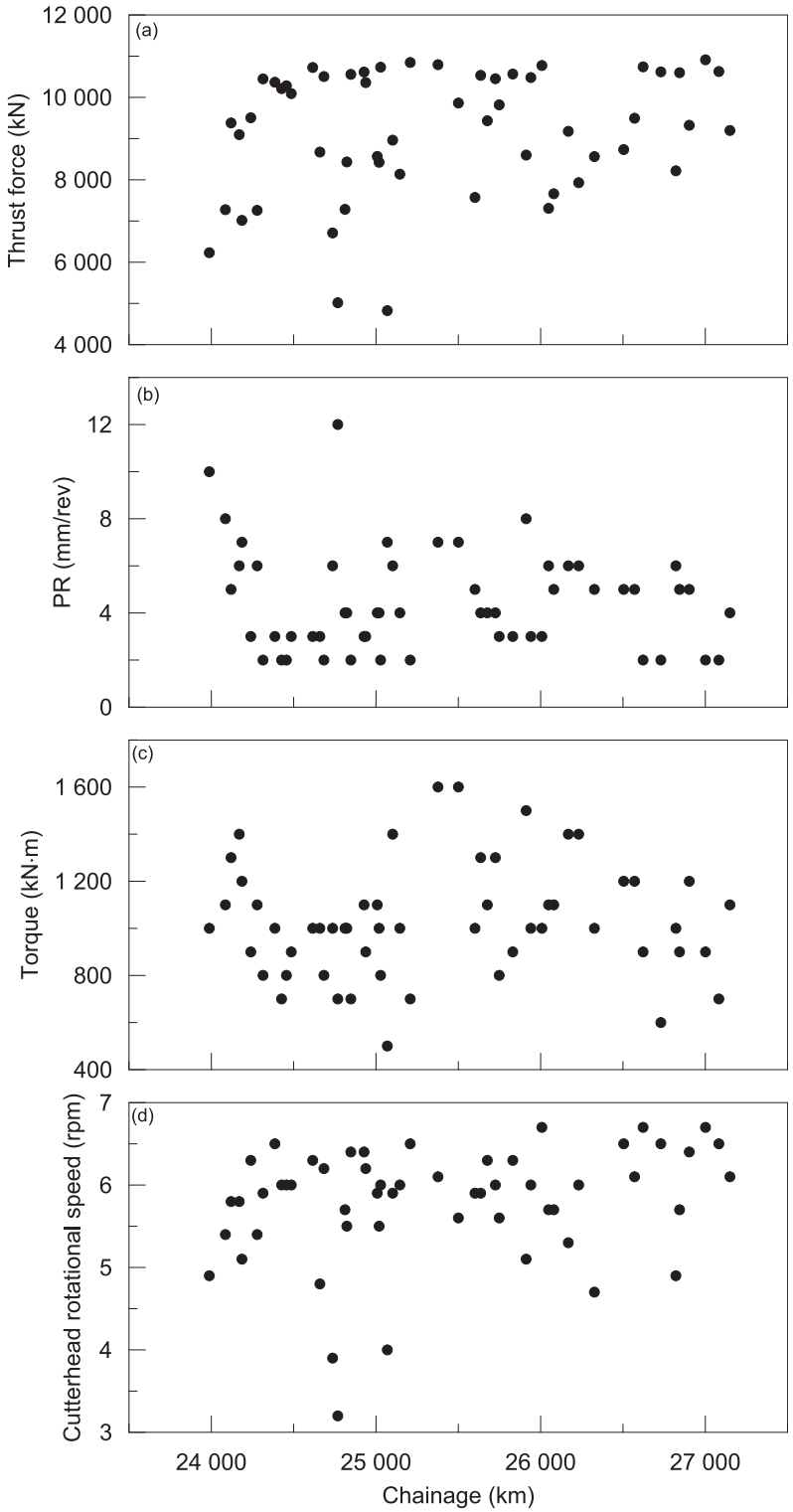

Fig. 4. Operational parameters of TBM in ET within the Central Gneiss unit. (a) Thrust force (kN), (b) PR (mm/rev), (c) torque (kN·m), and (d) cutterhead rotational speed (rpm).

are more scattered. The lower-left quadrant (Quadrant 3) includes models such as Innaurato et al. (1991) and Farrokh et al. (2012). These models exhibit both low R^2 and RMSE values, indicating random error behaviour. Finally, the lower-right quadrant (Quadrant 4), characterised by low R^2 and high RMSE values, contains the models exhibiting the least systematic and most random error behaviour. Notably, the Hassanpour et al. (2011)

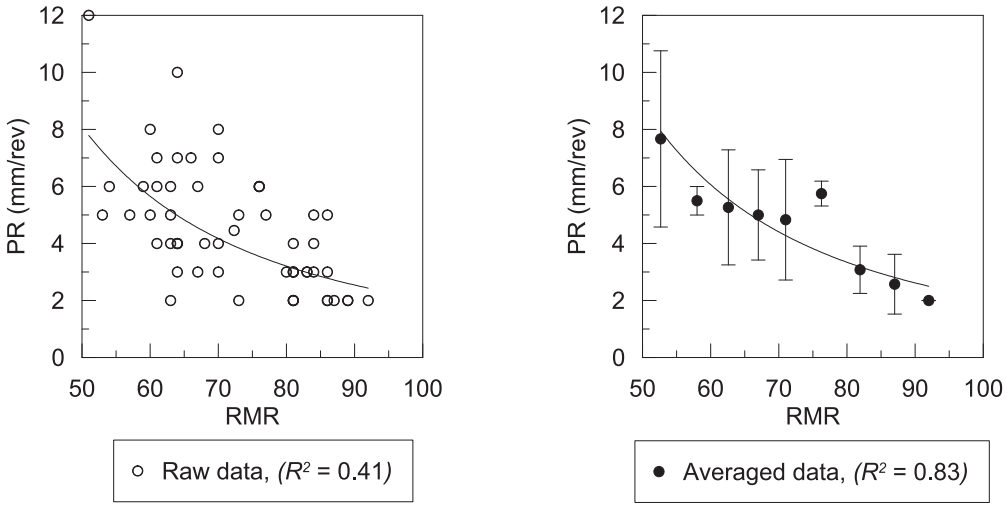

Fig. 5. Correlation between RMR and PR with raw (left) and averaged (right) datasets.

Table 5
Units used by different models for expressing penetration rates and appropriate unit conversions.

Original unit	Conversion to mm/rev	Model
m/h	(Original value × 1000)/(60 × v_{rot})	Cassinelli et al. (1982) Frough et al. (2015)
(mm/rev)/(MN/cutter)	Original value × F_N (kN/cutter) × 1000	Ribacchi and Lembo Fazio (2005)
(kN/cutter)/(mm/rev)	F_N (kN/cutter)/original value	Hamidi et al. (2010) Hassanpour et al. (2011) Kim et al. (2020)

Table 6
Measured and predicted mean penetration values.

		PR (mm/rev)
Measured		4.46
Predicted	Hassanpour et al. (2011) (UCS, RQD)	4.50
	Innaurato et al. (1991)	4.55
	Gehring (1995)	4.88
	Farrokh et al. (2012)	5.28
	Hassanpour et al. (2011) (RMR)	3.51
	Cassinelli et al. (1982)	3.49
	Ribacchi and Lembo Fazio (2005)	3.01
	Hamidi et al. (2010)	6.12
	Hassanpour et al. (2011) (GSI)	7.48
	Kim et al. (2020)	9.64
	Frough et al. (2015)	11.20

models based on RMR and GSI fall within this region, reflecting the high randomness of the results provided by such models. This performance highlights their inadequacy for reliable estimation of TBM penetration rates in the Central Gneiss unit.

Overall, this analysis emphasises the importance of selecting empirical models capable of providing low prediction errors with systematic behaviour, to ensure proper adaptation to the BBT case study. Among those evaluated, the models proposed by Cassinelli et al. (1982), Kim et al. (2020), and Ribacchi and Lembo Fazio (2005) consistently demonstrate good predictive performance for the Central Gneiss unit. However, the model of Ribacchi and Lembo Fazio (2005) shows a negative correlation coefficient between measured and estimated data, suggesting limited prediction ability when applied to the BBT case study.

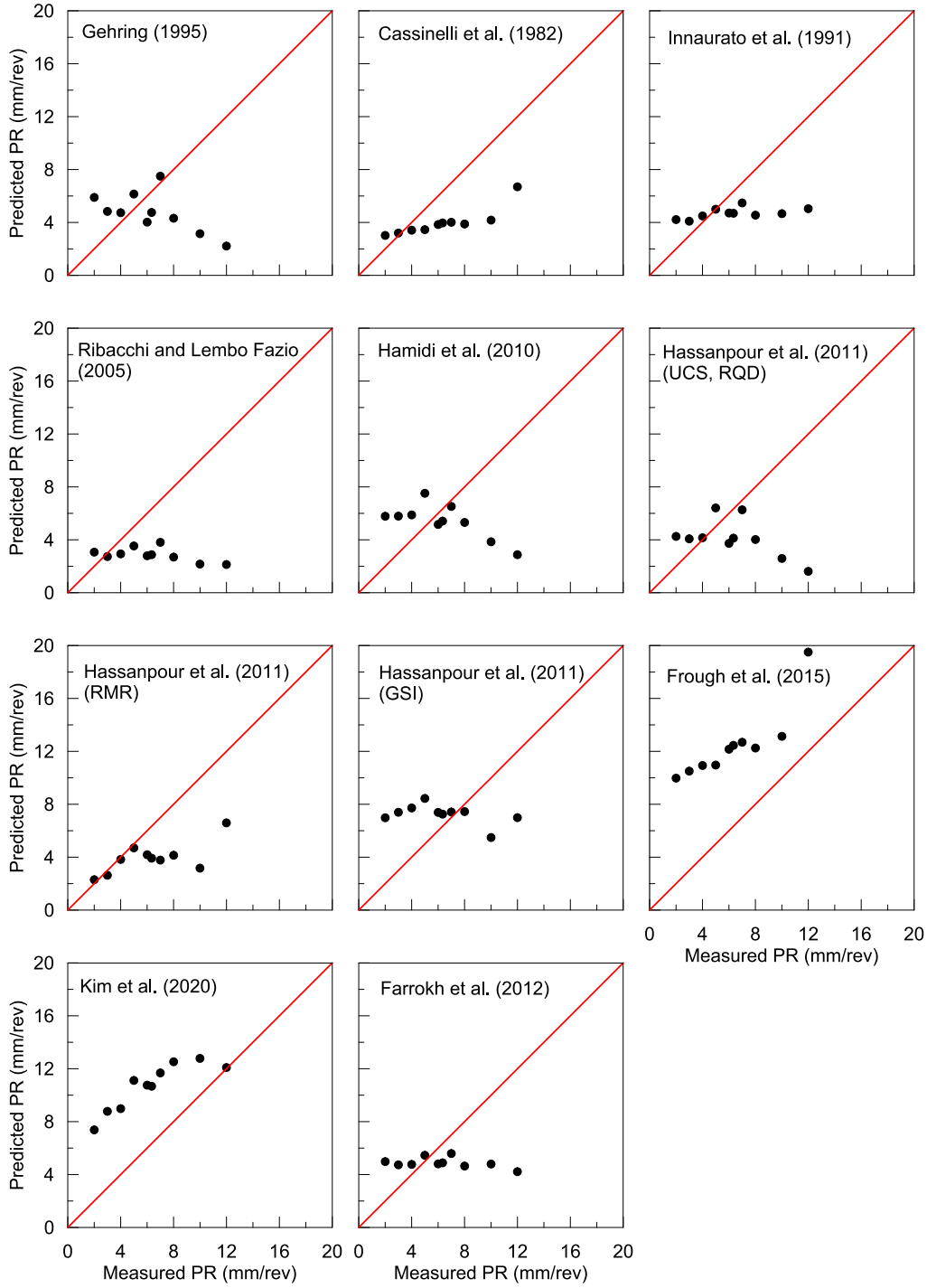

Fig. 6. Comparison of measured and predicted PR for various empirical TBM performance models.

4.3 RMR and GSI correlation analysis

Figure 9 illustrates the relationships between RMR and the various TBM performance parameters, while Fig. 10 presents the corresponding relationships with GSI. The PR exhibits an exponential decrease with increasing values of both RMR and GSI, indicating that higher-quality rock masses are associated with reduced TBM advance rates. This behaviour can be attributed to the greater strength and lower drillability of more competent rock masses. The trend of PR can be broadly described in three stages: a stand-alone peak at the lower end of the RMR and GSI ranges, a tendency towards stabilisation at intermediate values, and a marked decrease corresponding to the highest values of both indices.

The BI displays a nonlinear positive relationship with both RMR and GSI, following a similar pattern. This suggests that boreability is influenced by a combination

Table 7
Comparison of statistical indicators (RMSE and ρ) assessing the error between measured and predicted values for the various models.

Analysis of the models	RMSE	ρ
Cassinelli et al. (1982)	3.27	0.86
Innaurato et al. (1991)	3.32	0.56
Gehring (1995)	4.48	–0.62
Ribacchi and Lembo Fazio (2005)	4.85	–0.54
Hamidi et al. (2010)	4.23	–0.73
Hassanpour et al. (2011) (UCS, RQD)	4.63	–0.55
Hassanpour et al. (2011) (RMR)	3.41	0.70
Hassanpour et al. (2011) (GSI)	3.62	–0.46
Farrokh et al. (2012)	3.64	–0.46
Frough et al. (2015)	6.31	0.87
Kim et al. (2020)	4.68	0.88

of factors beyond rock mass classification alone. Notably, optimal boreability does not necessarily correspond to either the weakest or the strongest rock masses. A very low BI value is observed at the lower end of the GSI range, while the index appears more stable when considered in relation to low RMR values. The ICR reaches its maximum at low RMR and GSI values, and decreases as rock mass quality improves. An increase in ICR is also observed at intermediate RMR and GSI values, with a more distinct peak in relation to RMR. This pattern reflects the combined influence of rock mass breakability and TBM operational efficiency. The SE displays an increasing trend with both RMR and GSI, indicating that higher-quality rock masses require greater energy input per unit volume of excavated material. This reflects their higher resistance to mechanical breakage. The P exhibits a parabolic relationship with both RMR and GSI, tending to be lower at the extremes and reaching a maximum at intermediate values. This pattern likely results from the combined effects of machine load (thrust force and torque) and rock mass strength. In low-strength rock masses, the TBM encounters minimal resistance, facilitating excavation and reducing power demand. In contrast, although high-quality rock masses are stronger and more difficult to penetrate, they also lead to significantly reduced penetration rates, which in turn lowers overall power consumption. At intermediate RMR and GSI values, the TBM operates under higher thrust while maintaining a relatively high penetration rate, resulting in peak power consumption due to the greater energy required to fracture the rock. The SP shows a

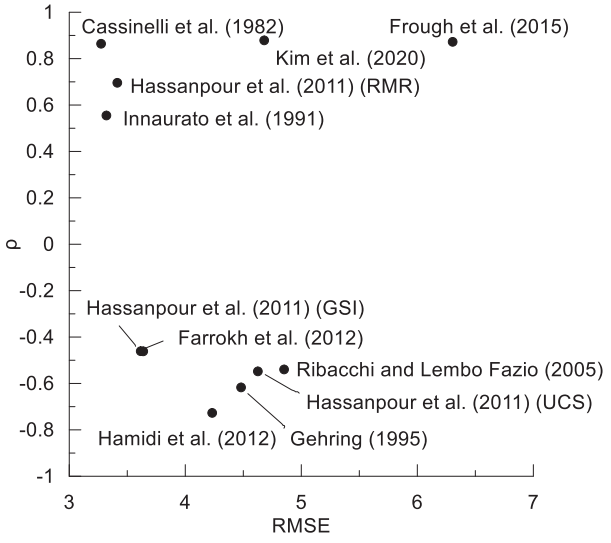

Fig. 7. Distribution of TBM performance prediction models based on RMSE and ρ values, obtained by comparing measured and predicted PR for each model.

Table 8
Coefficient of determination (R^2) and RMSE from linear and polynomial regressions applied to the prediction errors of the models.

Analysis of the error of the models	Linear regression		Polynomial regression	
	R^2	RMSE	R^2	RMSE
Cassinelli et al. (1982)	0.75	0.52	0.87	0.37
Innaurato et al. (1991)	0.31	0.34	0.45	0.30
Gehring (1995)	0.38	1.19	0.52	1.04
Ribacchi and Lembo Fazio (2005)	0.29	0.44	0.51	0.37
Hamidi et al. (2010)	0.53	0.89	0.77	0.62
Hassanpour et al. (2011) (UCS, RQD)	0.30	1.20	0.62	0.89
Hassanpour et al. (2011) (RMR)	0.48	0.86	0.49	0.85
Hassanpour et al. (2011) (GSI)	0.21	0.66	0.30	0.62
Farrokh et al. (2012)	0.21	0.38	0.43	0.33
Frough et al. (2015)	0.76	1.31	0.88	0.93
Kim et al. (2020)	0.77	0.85	0.96	0.37

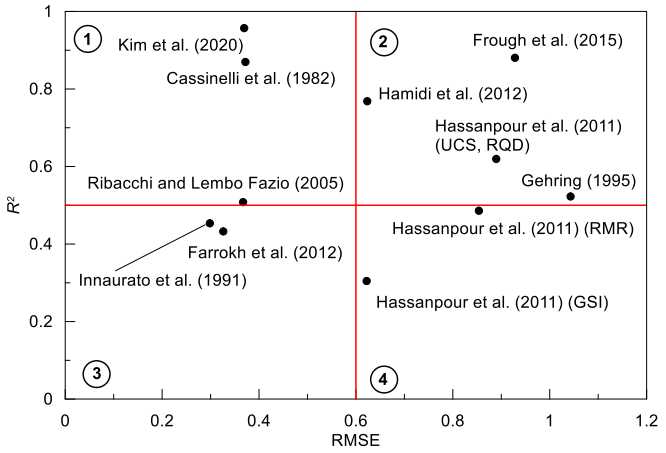

Fig. 8. Distribution of TBM performance prediction models based on RMSE and R^2 values derived from error analysis using second-order polynomial regression.

negative correlation with RMR and GSI, decreasing exponentially. This further confirms that as rock mass quality improves, TBM penetration efficiency declines.

Overall, the high R^2 obtained for most parameters confirms the strong correlation between both RMR and GSI and the key TBM performance indicators. These results highlight the significant influence of rock mass quality on TBM operational behaviour, with more competent rock masses generally resulting in lower penetration rates and higher energy consumption.

4.4 Comparison with preceding studies

The results of this study align with general trends reported in the literature regarding the use of RMR- and GSI-based models for TBM performance prediction (Frough et al., 2015; Benato & Oreste, 2015; Armetti et al., 2018; Paltrinieri et al., 2016). Both the present analysis and previous research consistently show that the PR of TBM decreases with increasing RMR and GSI values, while SE and P increase, reflecting the greater strength and reduced drillability of higher-quality rock masses (Celeda et al., 2009; Exadaktylos et al., 2008). However, a detailed comparison reveals that although literature models based on RMR and GSI provide a sound general framework, their direct application to the Central Gneiss unit, as considered here, tends to underestimate actual TBM performance and yields larger prediction errors. In contrast, the new RMR- and GSI-based regression models (Eqs. (6) and (7), respectively) are developed and calibrated with site-specific data in this study, demonstrating significantly improved prediction accuracy, as indicated by higher R^2.

$$\mathrm{PR} = 36.375 \cdot \mathrm{e}^{-0.03 \cdot \mathrm{RMR}} \left(R^2 = 0.83\right), \tag{6}$$

$$\mathrm{PR} = 41.419 \cdot \mathrm{e}^{-0.031 \cdot \mathrm{GSI}} \left(R^2 = 0.79\right). \tag{7}$$

These findings highlight the necessity of calibrating empirical models to local geological and operational conditions to achieve reliable performance forecasts. Overall, the strong agreement between the trends observed in this study and those in references confirms the applicability of RMR and GSI as key predictors, while emphasising the importance of project-specific refinement to optimise TBM performance prediction.

4.5 Application of exploratory tunnel observations to main tunnels

The RMR and GSI-based predictive models (Eqs. (6) and (7)) derived from the TBM performance assessment in the ET were applied to the MT-E and MT-W to evaluate their predictive accuracy in the same rock-mass (Fig. 11).

Figure 11 presents the relationship between the measured PR values in the main tunnels and the values predicted using the two equations derived from the ET based on the RMR and GSI data. The related error analysis is presented in Table 9.

The error analysis related to the application of two models (RMR- and GSI- based) to the main tunnels presents an RMSE of around 2.11 mm/rev, while the mean error reaches 0.89 mm/rev. Due to this, the systematic and casual errors have a similar impact: casual errors fluctuating around the regression curve contribute by 0.9 mm/rev (43%), while systematic errors, shifting the data away from the prediction curve, contribute by the remnant 1.2 mm/rev (57%). Analysing in detail the application of two models separately, Eq. (6) model (RMR based) is affected by bigger errors than the Eq. (7) model (GSI based), overall in terms of casual error around the regression curve. On the other hand, analyzing the behavior of two tunnels, the models perform in a similar way, without significant variations between them.

Combining the models and tunnels, the best result is given by Eq. (7) model (GSI based) over the MT-E, which shows the lowest values of both RMSE and mean error. On the other hand, the highest value of RMSE is provided for the Eq. (6) model (RMR based) over the MT-E, while the highest value of mean error is given for the same model, but applied over the MT-W. In any case, the differences among results are quite low.

The good agreement between the predicted and measured values indicates that the predictive models developed from the ET data can be reliably applied to the main tunnels in the same geological and geomechanical context. This agreement is particularly notable given the substantial differences in TBM type and main tunnel dimensions.

5 Conclusions

This study investigated TBM performance prediction in the BBT exploratory tunnel, focusing on the Central

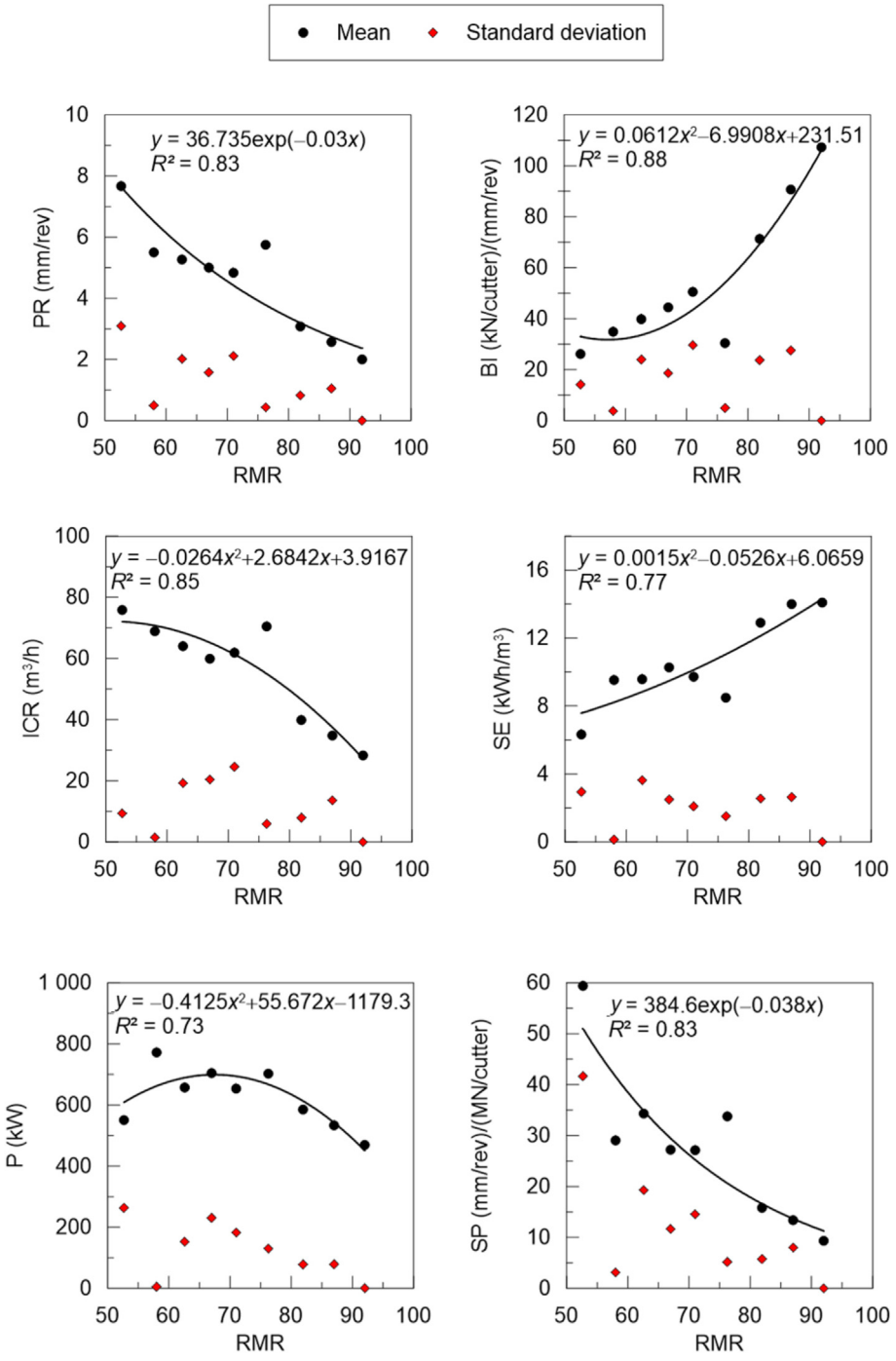

Fig. 9. Relationships between RMR and TBM performance parameters.

Gneiss unit, which is characterised by high strength and abrasiveness. By comparing several established empirical models with actual field data, the research identified the most accurate methods for estimating TBM operational parameters. Statistical analyses demonstrated that rock mass classification indices, particularly RMR and GSI, strongly correlated with key TBM performance metrics such as penetration rate, specific energy, and power consumption.

The newly developed predictive models based on RMR and GSI significantly improved the accuracy of performance estimation within the studied geological and geomechanical setting. These findings highlight the essential role of detailed geomechanical assessment in TBM project planning and execution and stress the importance of integrating site-specific data into performance prediction models.

The strong correlation between the estimated and observed values, particularly for critical parameters such

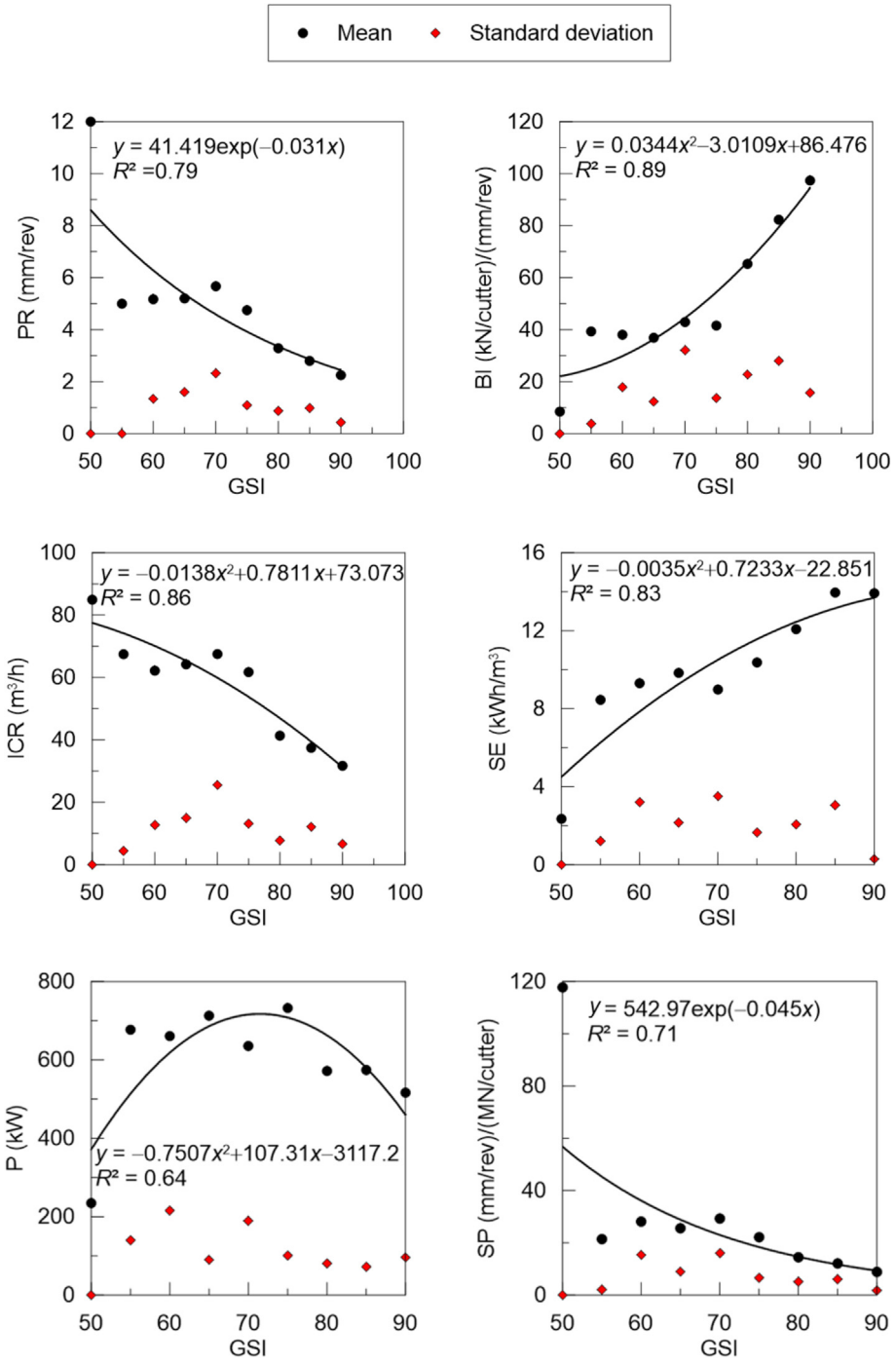

Fig. 10. Relationships between GSI and TBM performance parameters.

as PR, demonstrates the effectiveness of leveraging the ET findings to forecast and optimise the TBM performance in the main tunnels. The transferability and reliability of the predictive models developed in the ET setting are validated by their successful application to the main tunnel excavation. While the proposed models show significant promise in predicting TBM performance within the context of the Central Gneiss unit of the BBT, the direct transferability of these models to other projects in different geological settings should be approached with caution and will be the subject of further investigations. Ultimately, these results may support improved decision-making and resource management in projects involving similar ground conditions.

Table 9
Error analysis related to the application of the new developed to the main tunnels.

Model	Main tunnel	RMSE per tunnel	RMSE per model	RMSE	Mean error per tunnel	Mean error per model	Mean error
Eq. (6) model (RMR based)	MT-E	2.27	2.21	2.11	1.08	1.11	0.89
	MT-W	2.15			1.13		
Eq. (7) model (GSI based)	MT-E	1.94	2.00		0.53	0.67	
	MT-W	2.06			0.80		

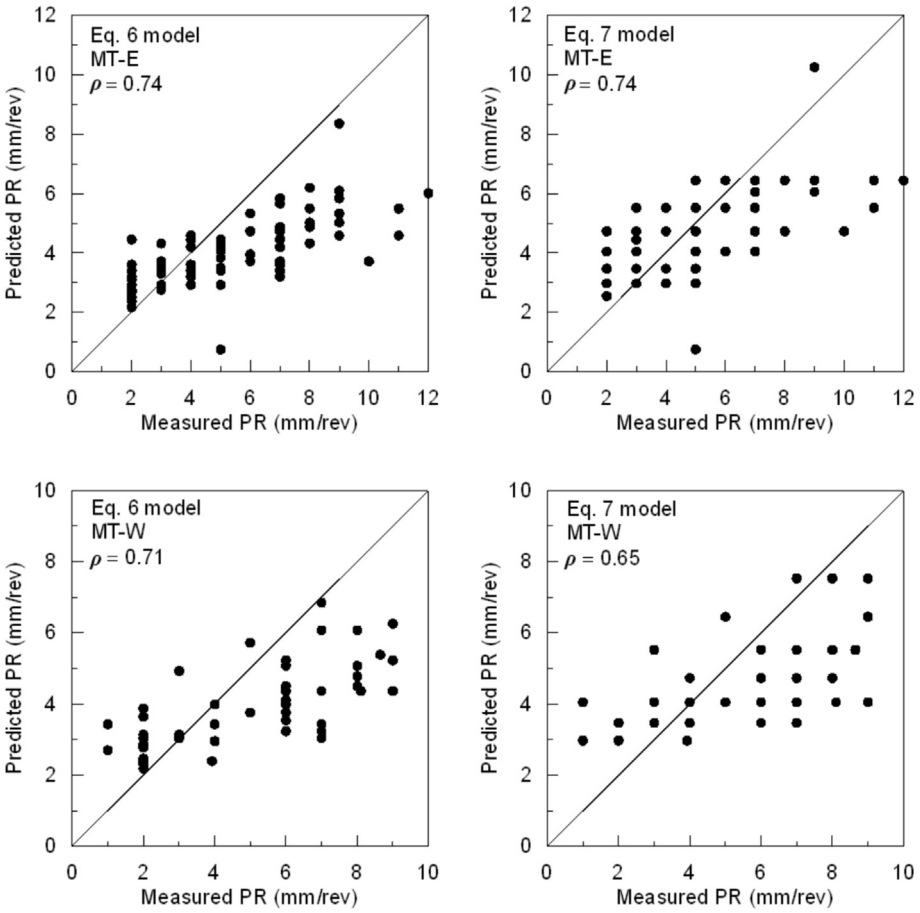

Fig. 11. Application of the developed penetration rate models to the main tunnels (MT-E and MT-W) and comparison between measured and predicted PR values.

Data availability

The data that support the findings of this study are available from the corresponding author upon reasonable request.

CRediT authorship contribution statement

Deniz Aydin: Writing – original draft, Investigation, Funding acquisition, Formal analysis. **Francesco Tinti:** Writing – original draft, Visualization, Supervision, Methodology. **Daniela Boldini:** Writing – review & editing, Visualization, Validation, Project administration, Methodology, Conceptualization.

Declaration of competing interest

Dr. Daniela Boldini is an associate editor for *Underground Space* and was not involved in the editorial review or the decision to publish this article. All authors declare that there are no competing interests.

Acknowledgement

The authors gratefully acknowledge the financial support provided to Deniz Aydin by the Scientific and Technological Research Council of Turkey.

Appendix A

k_2 = factor for rock mass fabric

Table A1
Correction factor k_2 as a function of discontinuity spacing and orientation relative to the tunnel axis in terms of the angle α (Wilfing, 2016).

Spacing of discontinuity	Correction factor k_2 at α (°)			
	0	30	60	90
<50 cm	1.0	1.0	1.0	1.0
10–50 cm	1.2	1.3	1.6	1.3
5–10 cm	1.4	1.8	2.3	1.6
>5 cm	1.7	2.3	3.0	2.0

Note: $\alpha = \sin^{-1}[\sin\alpha_f \times \sin(\alpha_t - \alpha_s)]$, where α denotes the smallest angle between tunnel axis and discontinuity (°); α_f denotes the dip angle discontinuity (°); α_s denotes the strike angle discontinuity (°); α_t denotes the tunnel direction (°).

k_3 = factor for state of stress in rock mass

Gehring was unable to define a correction factor for the stress field at the tunnel face and side walls, as his analysis was limited to tunnel projects with overburdens of less than 250 m, where no significant horizontal stress regime was anticipated. However, in major base tunnel projects crossing the Alps, instabilities at the tunnel face and side walls have been observed, frequently resulting in blocky faces. Consequently, in tunnel projects with greater overburden or a notable horizontal stress component, an influence on the penetration rate is to be expected. Nevertheless, a suitable formula to account for this influence has yet to be developed (Wilfing, 2016).

k_5 = factor for cutter spacing ≠ 80 mm.

This correction factor is derived from research conducted at NTNU on the relationship between cutter spacing and penetration. It has been demonstrated that, under constant thrust force, reduced cutter spacing results in higher penetration rates. The recommended correlation diagram for k_5 accounts for the effects of cutter spacing values differing from 80 mm, while also considering the cuttability of the rock (Wilfing, 2016).

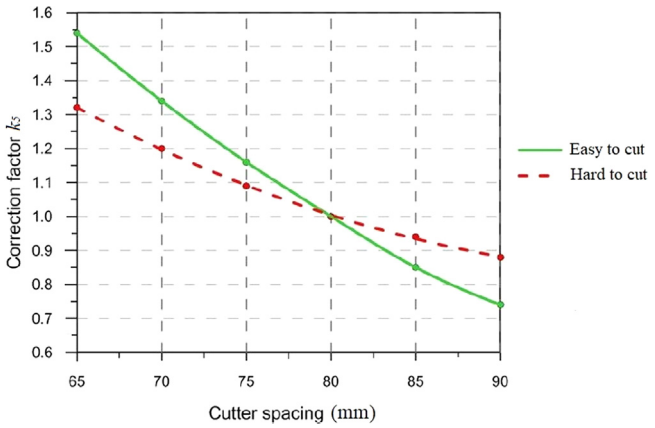

Fig. A1. Correlation diagram of correction factor k_5 and cutter spacing as a function of drillability (Wilfing, 2016).

Appendix B

Table B1
Code and corresponding values of the rock type code, RT_c (Farrokh et al., 2012).

Rock type	Code	RT_c
Claystone, mudstone, marl, slate, phyllite, and argillite	C	5
Sandstone, siltstone, conglomerate, and quartzite	S	3
Limestone, chalk, dolomite, and marble	L	3
Karstic limestone	K	3
Metamorphic rocks such as gneiss and schist	M	2
Coarse igneous such as granite and diorite	G	1
Fine volcanic such as basalt, tuff, and andesite	V	2

References

Alber, M. (2000). Advance rates of hard rock TBMs and their effects on project economics. *Tunnelling and Underground Space Technology, 15* (1), 55–64.

Armaghani, D. J., Mohamad, E. T., & Momeni, E. (2021). Predicting TBM performance using machine learning techniques: A comprehensive review. *Geotechnical and Geological Engineering, 39*(4), 1–23.

Ayawah, P. E. A., Sebbeh-Newton, S., Azure, J. W. A., Kaba, A. G. A., Anani, A., Bansah, S., & Zabidi, H. (2022). A review and case study of artificial intelligence and machine learning methods used for ground condition prediction ahead of tunnel boring machines. *Tunnelling and Underground Space Technology incorporating Trenchless Technology Research, 125*, 1–14.

Armetti, G., Migliazza, M., Ferrari, F., Berti, A., & Padovese, P. (2018). Geological and mechanical rock mass conditions for TBM performance prediction. The case of "La Maddalena" exploratory tunnel,

Chiomonte (Italy). *Tunnelling and Underground Space Technology, 77*, 115–126.
Azarafza, M., Hajialilue Bonab, M., & Derakhshani, R. (2022). A deep learning method for the prediction of the index mechanical properties and strength parameters of marlstone. *Materials, 15*, 6899.
Barton, N. (1999). TBM performance estimation in rock using Q_{TBM}. *Tunnels and Tunnelling International, 31*, 30–34.
Benato, A., & Oreste, P. (2015). Prediction of penetration per revolution in TBM tunneling as a function of intact rock and rock mass characteristics. *International Journal of Rock Mechanics and Mining Sciences, 74*, 119–127.
Bilgin, N., Copur, H., & Balci, C. (2014). *Mechanical excavation in mining and civil industries*. CRC Press.
Boldini, D., Bruno, R., Egger, H., Stafisso, D., & Voza, A. (2018). Statistical and geostatistical analysis of drilling parameters in the Brenner Base Tunnel. *Rock Mechanics and Rock Engineering, 51*, 1955–1963.
Brino, G., Peila, D., Steidl, A., & Fasching, F. (2015). Prediction of performance and cutter wear in rock TBM: Application to Koralm tunnel Project. *Georesources and Mining, 2*, 37–50.
Bruland, A. (1998). Hard rock tunnel boring: Performance predictions and cutter life assessments [Ph.D. Thesis, Norwegian University of Science and Technology].
Cassinelli, F., Cina, S., Innaurato, N., Mancini, R., & Sampaolo, A. (1982). Power consumption and metal wear in tunnel-boring machines: analysis of tunnel-boring operation in hard rock. In *Tunneling 82* (pp. 73–81). London: Institution of Mining and Metallurgy.
Celeda, B., Galera, J. M., Munoz, C., & Tardaquila, I. (2009). The use of the specific drilling energy for rock mass characterization and TBM driving during tunnel construction. In *ITA-AITES World Tunnel Congress 2009* (pp. 1–13). Budapest, Hungary: Hungarian Tunnelling Association.
Cemiloglu, A., Zhu, L., Arslan, S., Xu, J., Yuan, X., Azarafza, M., & Derakhshani, R. (2023). Support Vector Machine (SVM) application for uniaxial compression strength (UCS) prediction: A case study for maragheh limestone. *Applied Sciences, 13*, 2217.
Egger, H., Foderà, M. G., Gianluca Liuzzi, G., Spaziani, A., Voza, A., & Boldini, D. (2023). Performance of different diameter double shield TBMs: Experiences from excavation of exploratory tunnel and main tubes of the Italian lot mules 2–3 Brenner Base Tunnel. In *15th ISRM Congress 2023 & 72nd Geomechanics Colloquium* (pp. 63–68). Salzburg, Austria: CRC Press.
Entacher, M., & Rostami, J. (2019). TBM performance prediction model with a linear base function and adjustment factor obtained from rock cutting and indentation tests. *Tunnelling and Underground Space Technology, 93*, 1–13.
Exadaktylos, G., Stavropoulou, M., Xiroudakis, G., de Broissia, M., & Schwarz, H. (2008). A spatial estimation model for continuous rock mass characterization from the specific energy of a TBM. *Rock Mechanics and Rock Engineering, 41*, 797–894.
Farrokh, E., Rostam, J., & Laughton, C. (2012). Study of various models for estimation of penetration rate of hard rock TBMs. *Tunnelling and Underground Space Technology, 30*, 110–123.
Frough, O., Torabi, S. R., & Yagiz, S. (2015). Application of RMR for estimating rock-mass-related TBM utilization and performance parameters: A case study. *Journal of Rock Mechanics and Geotechnical Engineering, 48*, 1305–1312.
Gehring, K. H. (1995). Leistungs- und Verschleißprognosen im maschinellen Tunnelbau. *Felsbau, 13*, 439–448 (in German).
Goodarzi, A. R., Taheri, A., & Jalalifar, H. (2021). TBM performance prediction in complex geological conditions: A review of current practices. *Journal of Rock Mechanics and Geotechnical Engineering, 13* (2), 348–366.
Hamidi, J. K., Shahriar, K., Rezai, B., & Rostami, J. (2010). Performance prediction of hard rock TBM using Rock Mass Rating (RMR) system. *Tunnelling and Underground Space Technology, 25*, 333–345. https://doi.org/10.1016/j.tust.2010.01.008.
Hassanpour, J., Rostami, J., & Zhao, J. (2011). A new hard rock TBM performance prediction model for project planning. *Tunnelling and Underground Space Technology, 26*(5), 595–603.
Innaurato, N., Mancini, A., Rondena, E., & Zaninetti, A. (1991). Forecasting and effective TBM performances in a rapid excavation of a tunnel in Italy. In *7th ISRM Congress* (pp.1009–1014). Aachen, Germany.
Jing, L.-J., Li, J.-B., Yang, C., Chen, S., Zhang, N., & Peng, X.-X. (2019). A case study of TBM performance prediction using field tunnelling tests in limestone strata. *Tunnelling and Underground Space Technology, 83*, 364–372. https://doi.org/10.1016/j.tust.2018.10.001.
Kim, K. Y., Jo, S. A., Ryu, H. H., & Cho, G. C. (2020). Prediction of TBM performance based on specific energy. *Geomechanics and Engineering, 22*(6), 489–496.
Liu, Q. S., Liu, J. P., Pan, Y. C., Kong, X. X., & Hong, K. R. (2017). A case study of TBM performance prediction using a chinese rock mass classification system—hydropower classification (HC) method. *Tunnelling and Underground Space Technology, 65*, 140–154.
Maggio, G., Voza, A., & Egger, H. (2022). Key machine parameters for classification of rock mass in TBM excavation in BBT. In *World Tunnel Congress 2022* (pp. 9). Copenhagen, Denmark.
Naghadehi, M. Z., Samaei, M., Ranjbarnia, M., & Nourani, V. (2018). State-of-art predictive modeling of TBM performance in changing geological conditions through gene expression programming. *Measurement, 126*, 46–57.
Nelson, P. P., & O'Rourke, T. D. (1983). Field penetration index for TBM performance prediction. *Proceedings of the Rapid Excavation and Tunneling Conference, 2*, 823–845.
Paltrinieri, E., Sandrone, F., & Zhao, J. (2016). Anaylsis and estimation of gripper TBM performances in highly fractured and faulted rocks. *Tunnelling and Underground Space Technology, 52*, 44–61. https://doi.org/10.1016/j.tust.2015.11.017.
Pourhashemi, S. M., Ahangari, K., Hassanpour, J., & Eftekhari, S. M. (2021). Evaluating the influence of engineering geological parameters on TBM performance during grinding process in limestone strata. *Bulletin of Engineering Geology and the Environment, 80*, 3023–3040.
Ribacchi, R., & Lembo-Fazio, A. (2005). Influence of rock mass parameters on the performance of a TBM in a Gneissic formation (Varzo tunnel). *Rock Mechanics and Rock Engineering, 38*(2), 105–127.
Rostami, J., & Ozdemir, L. (1993). A new model for performance prediction of hard rock TBM. In *RETC 1993: Rapid Excavation and Tunneling Conference* (pp. 793–809). Boston, MA: Society for Mining, Metallurgy, and Exploration.
Salimi, A., Rostami, J., Moormann, C., & Hassanpour, J. (2022). Introducing tree based regression models for prediction of hard rock TBM performance with consideration of rock type. *Rock Mechanics and Rock Engineering, 55*, 4869–4891.
Sapigni, M., Berti, M., Behtaz, E., Busillo, A., & Cardone, G. (2002). TBM performance estimation using rock mass classification. *International Journal of Rock Mechanics and Mining Sciences, 39*(6), 771–788.
She, Y., Zhang, J., & Liu, Q. (2024). Recent advancements in TBM technology and its applications in urban tunneling. *Tunnelling and Underground Space Technology, 134*, 104–115.
Tinti, F., Spaggiari, C., Lanconelli, M., Voza, A., & Boldini, D. (2023). Exploitation of drainage water heat: A novel solution experimented at the Brenner Base Tunnel. *Tunnelling and Underground Space Technology, 137*, 105131.
Wilfing, L. Z. F. (2016). *The influence of geotechnical parameters on penetration prediction in TBM tunneling in hard rock* [Doctoral dissertation, Technical University of Munich].
Yagiz, S. (2003). A model for the prediction of TBM performance in hard rock condition [Paper presentation]. In *56th Geological Congress of Turkey*, Ankara, Turkey.
Yalei, Y., Lijie, D., Rong, T., Fei, W., & Huilan, Z. (2024). Prediction of TBM penetration rate for different surrounding rocks and cutter head diameters. *Heliyon, 10*, 1–14.
Yan, W., Liu, S., & Wang, Z. (2024). The role of geological variability in TBM performance prediction: A case study. *Engineering Geology, 312*, 106–120.
Yang, W., Chen, Z., Zhao, H., Chen, S., & Shi, C. (2025a). Feature fusion method for rock mass classification prediction and interpretable analysis based on TBM operating and cutter wear data. *Tunnelling and Underground Space Technology, 157*, 106351.
Yang, W., Chen, Z., Wang, S., Zhao, H., Li, J., Chen, S., & Shi, C. (2025b). Improved boreability index for gripper TBMs in medium- to strong-quality rocks based on theoretical analysis and field penetration tests. *Rock Mechanics and Rock Engineering, 58*, 5429–5453.